Local Glass Transition Temperature $T_{\rm g}(z)$ Within Polystyrene Is Strongly Impacted by the Modulus of the Neighboring PDMS Domain

Yannic J. Gagnon and Connie B. Roth*

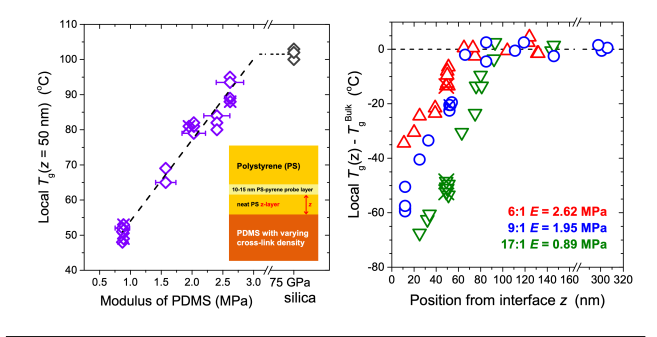
Department of Physics, Emory University, Atlanta, Georgia, 30322 USA

E-mail: cbroth@emory.edu

Submitted to ACS Macro Letters, Sept. 11, 2020; revised manuscript accepted Oct. 23, 2020.

This is the accepted version of the article. This article may be downloaded for personal use only. Any other use requires prior permission of the author and ACS Publications. This article appeared in *ACS Macro Letters* and may be found at https://doi.org/10.1021/acsmacrolett.0c00659.

ABSTRACT: Profiles in the local glass transition temperature $T_{\rm g}(z)$ within polystyrene (PS) next to polydimethylsiloxane (PDMS) domains were determined using a localized fluorescence method. By changing the base to cross-linker ratio, we varied the cross-link density and hence Young's modulus of PDMS (Sylgard 184). The local $T_{\rm g}(z)$ in PS at a distance of z = 50 nm away from the PS/PDMS interface was found to shift by 40 K as the PDMS modulus was varied from 0.9–2.6 MPa, demonstrating a strong sensitivity of this phenomenon to the rigidity of the neighboring domain. The extent the $T_{\rm g}(z)$ perturbation persists away from the PS/PDMS interface, $z \approx 65$ –90 nm before bulk $T_{\rm g}$ is recovered, is much shorter for this strongly immiscible system compared with the weakly immiscible systems studied previously, which we attribute to a smaller interfacial width as the χ parameter for PS/PDMS is an order of magnitude larger.



High performance multicomponent materials have nanostructured morphologies where the de-

sired global properties are obtained from an amalgam of local property changes caused by the multitude of internal interfaces. Studies on thin polymer films have demonstrated a host of property changes with decreasing film thickness attributed to interface effects, including polymer-polymer interfaces. The efficient design of multicomponent materials requires the understanding of how these interface effects perturb local properties. Glassy-rubbery interfaces between polymer domains impart material toughness and flexibility, 1920 and can be used to tune phononic transport. 211 Although a range of different processing methods have been developed to create morphologies with sub-100 nm domain sizes, 22-25 studies of simplified systems with a single interface can directly inform the underlying mechanisms behind such applications by mapping local properties as a function of distance from the interface.

In 2015, Baglay and Roth mapped how the local glass transition temperature $T_{\rm g}(z)$ changed across a glassy-rubbery polystyrene ($\dot{P}S$) / poly(nbutyl methacrylate) (PnBMA) interface, finding this profile in local dynamics to be much broader and asymmetric relative to the composition profile, 16 with follow-up work demonstrating a similar behavior for a range of weakly immiscible polymer pairs. The range the dynamical perturbation persisted away from the dissimilar polymerpolymer interface before bulk $T_{\rm g}$ was recovered for these semi-infinite bilayer systems depended on whether the neighboring polymer domain had a higher $T_{\rm g}^{\rm bulk}$ ("hard confinement"), extending to $z\approx 100$ –125 nm, or lower $T_{\rm g}^{\rm bulk}$ ("soft confinement"), extending to $z\approx 225$ –250 nm. An important observation from these studies was that these broad $T_{\rm g}(z)$ profiles only formed upon annealing the dissimilar polymer interface to equilibrium, suggesting that some factor during polymerpolymer interface formation was responsible for

the coupling of $T_{\rm g}$ dynamics across the interface. More recent work has identified that chain connectivity across the interface appears to play a dominant role, as opposed to interfacial roughness. However, a number of open questions remain: Does the breadth of the compositional interface impact the range of the dynamical $T_{\rm g}(z)$ perturbation? Is the modulus of the neighboring domain an important factor in dictating the $T_{\rm g}(z)$ response?

In the present work we test both these open questions by experimentally measuring the $T_{\rm g}(z)$ profile in PS next to polydimethylsiloxane (PDMS) by varying cross-link density to alter the modulus of the PDMS neighboring domain without changing the chemistry of the dissimilar polymer interface. A localized fluorescence method is used to measure the local $T_{\rm g}(z)$ of a thin pyrene-labeled PS probe layer placed at a distance z from the PS/PDMS interface. These findings demonstrate that the breadth of the compositional interface between the two dissimilar polymers and the modulus of the neighboring domain are key factors controlling the $T_{\rm g}(z)$ behavior, providing insight for related theoretical efforts in the field 1813 14 29 34 into the control parameters responsible for this phenomenon. Characterization of the local properties near the interface of PS/PDMS, in particular, are relevant for a range of applications from mechanical reinforcement of polymers 1920 to the buckling-based metrology used to measure the modulus of ultrathin glassy films. 35-37

Figure 1a illustrates the multilayer sample geometry assembled for the fluorescence measurements that places a 10-15 nm thick pyrene-labeled PS probe layer ($M_{\rm w}=672$ kg/mol, $M_{\rm w}/M_{\rm n}=1.3,\,1.4$ mol% pyrene 161172738) at a known distance z from the PS/PDMS interface by changing the thickness z of a neat PS ($M_{\rm w}=1920~{\rm kg/mol},~M_{\rm w}/M_{\rm n}=$ 1.26) spacer layer between the underlying PDMS and pyrene-probe layer. An additional thick (>500 nm) neat PS layer is placed atop the probe layer to eliminate $T_{\rm g}$ shifts caused by the free surface. Layer thicknesses were measured using ellipsometry. By assembling samples with different z-layer thicknesses, the local $T_{\rm g}(z)$ value can be mapped out as a function of distance from the PS/PDMS interface. We ensure that the PS/PDMS interface is annealed to equilibrium by first assembling the z-spacer layer atop the PDMS and annealing these two layers for 90 min at 140 °C before adding the remaining layers. The entire multilayer stack is further annealed for 20 min at 120 °C immediately prior to the start of the fluorescence measurements to ensure thermal history has been erased, and to consolidate all the layers into a continuous material while still maintaining the morphology of the assembled structure shown in Fig. 1a. 16 High molecular weight polymers have been used to limit the diffusion of the pyrene-labeled probe

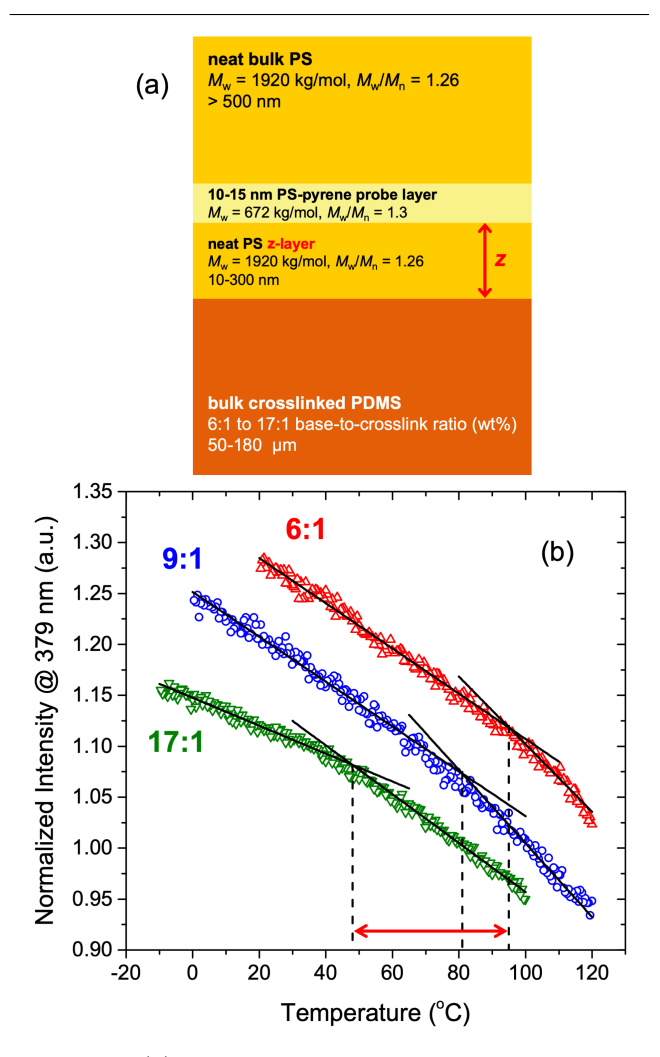


Figure 1. (a) Schematic of sample geometry assembled to place the 10-15 nm thick pyrene-labelled PS (PS-Py) probe layer at a distance z from the PS/PDMS interface by varying the thickness z of the neat PS spacer layer. (b) Temperature dependence of fluorescence intensity of PS-probe layer at z=50 nm for all three samples of varying PDMS cross-link density: $T_{\rm g}(z=50~{\rm nm})=48\pm2~{\rm ^{\circ}C}$ (17:1), $81\pm2~{\rm ^{\circ}C}$ (9:1), and $95\pm2~{\rm ^{\circ}C}$ (6:1).

layer and keep it localized at the position z by making the reptation time longer than the measurement time. PDMS layers (50–180 μ m thick) were made from Sylgard 184 (Dow Corning) where the base to cross-linker ratio was varied from 6:1 to 17:1 by weight and cured at 70 °C for 2 h following Refs. 35,40. The same $T_{\rm g}(z)$ values were also obtained for samples with 2 μ m thick PDMS layers formed by spin-coating, prior to curing under the same conditions. Thus, the measured $T_{\rm g}(z)$ values are independent of the thickness of the PDMS layer. Further experimental details are provided in the Supporting Information along with various control measurements.

Fluorescence measurements to determine the local $T_{\rm g}(z)$ were done on cooling at 1 °C/min by monitoring the pyrene emission intensity at a wave-

length of 379 nm for 3 s every 27 s, exciting at a wavelength of 330 nm. The temperature dependence of the fluorescence intensity is shown in Fig. 1b for three representative samples with varying PDMS cross-link densities, where the pyrene probe layer has been placed at a distance z = 50nm. Following previous works, 4115-117126127 the glass transition temperature $T_{\rm g}(z)$ is determined from the intersection of linear fits to the data above and below the transition. It is well known that pyrene fluorescence is extremely sensitive to the local environment's polarity, density, and rigidity, where the temperature dependence of the fluorescence intensity of pyrene within a polymer matrix reflects changes in the quantum yield of the dye due to the local rigidity of the surrounding matrix that is influenced by the polymer's thermal expansivity. 411-433 As established by Torkelson and co-workers, 4443 the T_{g} values from fluorescence agree well with ellipsometry and differential scanning calorimetry (DSC) for bulk samples. For the intensity vs. temperature curves shown in Fig. [1]b, the glass transition temperatures for these three samples are $T_{\rm g}(z=51~{\rm nm})=95\pm2~{\rm ^{\circ}C}$ for PDMS with 6:1 base to cross-linker ratio, $T_{\rm g}(z=53~{\rm nm})=81\pm2$ °C for 9:1, and $T_{\rm g}(z=51~{\rm nm})=48\pm2$ °C for 17:1. These data demonstrate that the local $T_g(z)$ of PS at z=50 nm is strongly reduced relative to the bulk $T_{\rm g}$ value for PS of $T_{\rm g}^{\rm bulk}=101.5\pm2.0$ °C and extremely sensitive to the properties of the neighboring PDMS layer, with the $T_{\rm g}(z=50~{\rm nm})$ values shifting by approximately 45 K as the PDMS base to cross-linker ratio is varied from 6:1 to 17:1.

The PDMS underlayers were fabricating using Dow Corning's Sylgard 184 elastomer kit by mixing the base prepolymer with the curing agent at different ratios n to create PDMS with different crosslink densities. Sylgard 184 has frequently been used in this manner with several groups characterizing the resulting modulus. To Figure we plot the Young's modulus E as a function of base to cross-linker ratio n measured by these various studies that used comparable curing conditions to our own, 70 °C for 2 h. Remarkable consistency is found for the measurements of Young's modulus E(n) using a range of different methods: tensile, E(n) and E(n) and E(n) and E(n) are the properties of th

$$E(n) = E_0 \exp\left(-\frac{n}{n_0}\right) \text{ (in MPa)},$$
 (1)

where $E_0 = 4.73 \pm 0.36$ MPa and $n_0 = 10.16 \pm 0.67$. Equation $\boxed{1}$ gives values for the PDMS modulus of $E = 0.89 \pm 0.12$ MPa for 17:1, $E = 1.95 \pm 0.19$ MPa for 9:1, and $E = 2.62 \pm 0.22$ MPa for 6:1. For the data shown in Fig. $\boxed{1}$, this implies that a

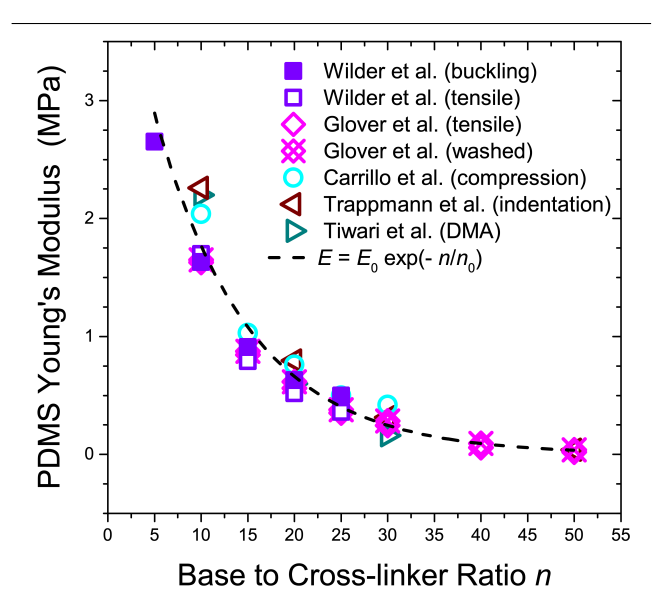


Figure 2. PDMS Young's modulus E for Sylgard 184 as a function of base to cross-linker ratio n measured using different methods as compiled from literature: Wilder et al., Glover et al., Carrillo et al., Trappmann et al., and Tiwari et al., Glover et al.'s data marked as X-diamonds represent samples washed in good solvent to extract unreacted small molecules.

change of the PDMS modulus by nearly a factor of three generated an approximately 45 K shift in the local $T_{\rm g}$ in PS at a distance of $z \approx 50$ nm from the PS/PDMS interface. We explore this trend more fully in Figure 3 by plotting the local $T_g(z = 50 \text{ nm})$ as a function of PDMS modulus for a range of different samples, using eq. 1 to determine E for the given base to cross-linker ratio nused. The trend in $T_{\rm g}(z=50~{\rm nm})$ with E appears linear, showing a large decrease in $T_{\rm g}(z=50~{\rm nm})$ of more than 20 °C/MPa with decreasing PDMS modulus in the range of E = 0.9-2.6 MPa, suggesting that the modulus of the neighboring domain is a dominant factor influencing the properties of PS. Interestingly, the value of $T_{\rm g}(z=50~{\rm nm})$ for the 6:1 ratio, when the PDMS modulus is still only E=2.6MPa, is already at 90.7 ± 3.3 °C, close to the bulk value for PS of $T_{\rm g}^{\rm bulk} = 101.5 \pm 2.0$ °C. For comparison, if we perform the same local $T_g(z = 50 \text{ nm})$ measurement in PS when the underlying material is silica (a material with a modulus 48 of ≈ 75 GPa), we obtain a local $T_g(z = 50 \text{ nm}) = 101.7 \pm 1.5 \text{ °C}$ as shown in Fig. 3, equivalent to $T_{\rm g}^{\rm bulk}$ as expected given that PS/silica is known to be a neutral interface not impacting the local $T_{\rm g}$ as measured by fluorescence. 4127,28 However, a comparison between the PS/PDMS system, where interdiffusion of the two polymers has been allowed to occur, with the PS/silica interface, where no such interdiffusion is possible, may not be the most pertinent.

In our group's 2017 study, we learned that the

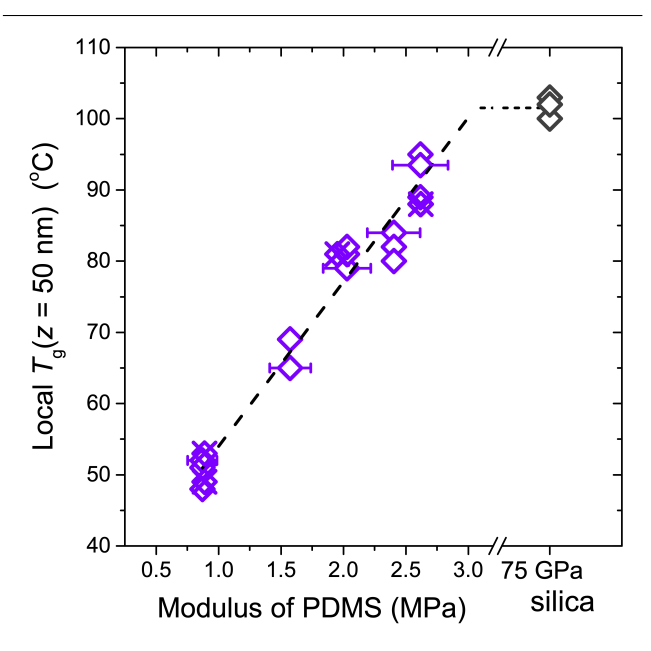


Figure 3. Local $T_{\rm g}(z)$ in PS at a fixed distance of z=50 nm from the PS/PDMS interface as a function of PDMS Young's modulus E, based on eq. (1). Representative horizontal error bars denote the uncertainty in E, while the symbol size indicates the vertical uncertainty of ± 2 °C in any given $T_{\rm g}$ measurement. The X-diamond symbols correspond to samples where the PDMS was washed in toluene, a good solvent, to extract unreacted small molecules. Grey diamonds at 75 GPa are $T_{\rm g}(z=50$ nm) for PS supported on silica with the horizontal dotted line corresponding to $T_{\rm g}^{\rm bulk}$.

interaction between the two polymer domains that creates the broad $T_{\rm g}(z)$ profile only occurs upon annealing of the dissimilar polymer-polymer interface to equilibrium. Local interpenetration of the two polymer domains at the interface is key to creating this coupling of dynamics that impacts the local properties over an extended distance from the interface. In follow-up work, we were able to show that chain connectivity plays a dominant role in this behavior, ²⁷ while interface roughness has little to no impact. However, it is worth noting that although chain connectivity across the interface itself seems to be important to at least create interfacial breadth, we are observing significant shifts in local $T_{\rm g}(z)$ at distances z sufficiently far away from the interface that no individual chain can span the distance. Shown in Supporting Information, we demonstrate how the $T_g(z = 50 \text{ nm})$ decrease develops upon annealing of the PS/PDMS interface at 140 °C, requiring 60–90 min to reach equilibrium. All $T_{\rm g}(z)$ measurements shown in Figs. 1, 3, and 4 are for samples where the PS/PDMS interface was annealed for 90 min at 140 °C to ensure equilibrium was reached. In the bucklingbased metrology method used to measure the elastic modulus of PDMS in Fig. 2 40 bilayer films of glassy PS atop rubbery PDMS are formed at room

temperature by stretching the PDMS layer prior to placing the glassy PS layer on top. Upon release of this initial strain, the PDMS layer contracts and the glassy PS layer buckles with an undulation wavelength that depends on the modulus of both layers. 35,36,40 In this measurement, because the PS/PDMS bilayer film is never heated above room temperature, there will be little to no interpenetration between the two polymer domains. Thus, we would not expect local $T_g(z)$ changes near the PS/PDMS interface, and would anticipate the PDMS modulus to be equivalent to bulk measurements as shown in Fig. 2. Interestingly, Vogt and coworkers have correlated a softening of the top glassy layer measured using the bucklingbased metrology method as the $T_{\rm g}$ of the glassy layer is approached. 349 Forrest and Dalnoki-Veress have shown that some limited interdiffusion can occur at glassy-rubbery interfaces below the $T_{\mathfrak{g}}$ of the glassy polymer. 50 Thus, it is possible that as the glassy $T_{\rm g}$ is approached from below, some limited interdiffusion is occurring at the glassy-rubbery interface between the glassy polymer layer and the underlying PDMS in the buckling-based metrology, resulting in an additional source of softening for the glassy layer.

One of the concerns with using the commercial Sylgard 184 elastomer kit is that the base and curing parts also contain additional components such as a catalyst, an inhibitor, solvent diluents, and silica filler (according to the product safety data sheets), 51152 which could affect the PDMS material formed. In addition, curing the material at a different base to cross-linker ratio from the recommended 10:1 ratio can result in unreacted small molecules still being present in the PDMS material after curing. This has been reported to be especially pronounced for n > 30, but for the range of $6 \le n \le 17$ used in our study, the percentage of unreacted mass is only $\sim 4-8$ %. Washing of the PDMS with a good solvent like toluene or heptane to swell the PDMS elastomer can be used to extract this unreacted material and other free small molecules. 44,51,52 Glover et al. 44 compared the modulus E(n) of Sylgard 184 PDMS before and after solvent washing to extract unreacted material and found only a very small difference in the modulus E for the range of n's shown in Fig. 2 (their washed E(n) values are denoted with X-diamond symbols). Perhaps a bigger concern for our $T_{\rm g}(z)$ measurements is that such free small molecules could migrate to the surface of PDMS and across to the PS domain, possibly causing plasticization of the material. We have verified that this concern is not impacting the measured $T_{\rm g}(z)$ values by washing our PDMS samples in toluene to remove such unreacted free material and confirmed that we obtain the same $T_{\rm g}(z)$ values pre- and postextraction. We show these measured $T_{\rm g}(z)$ values for samples where the PDMS layer has been washed in Fig. 3 with X-diamond symbols. Thus, we have ensured that the reduction in local $T_{\rm g}(z)$ near the PS/PDMS interface is not caused by plasticization, which is consistent with our earlier publication where we also demonstrated that the local $T_{\rm g}(z)$ profiles reported were not caused by plasticization from some low molecular weight component. 26

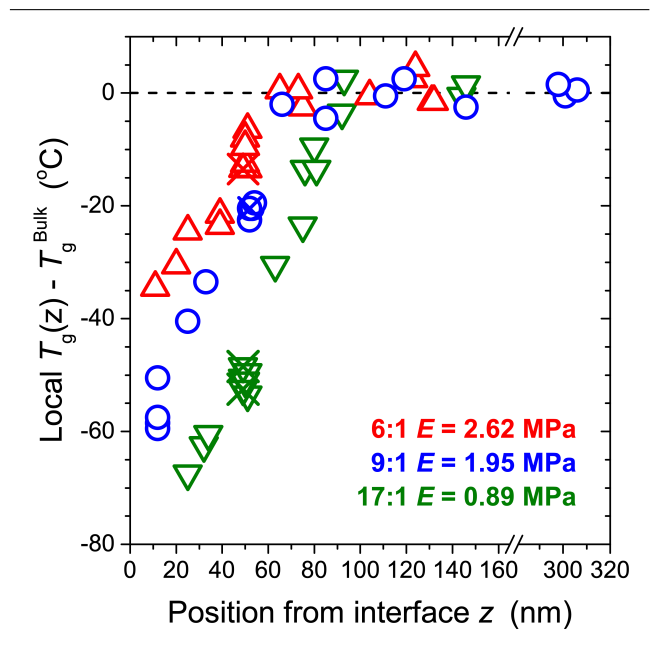


Figure 4. Local $T_{\rm g}(z)$ profile within PS as a function of distance z from the PS/PDMS interface for PDMS with three different cross-link densities (moduli). PS $T_{\rm g}^{\rm bulk}$ is recovered at $z\approx 65$ –90 nm. Data marked with an X denote samples where the cured PDMS was solvent washed to remove any unreacted monomer or impurities. Symbol size represents the ± 2 °C uncertainty associated with any given $T_{\rm g}$ measurement.

In Figure 4, we plot the $T_{\rm g}(z)$ profile within PS next to PDMS with varying cross-link densities: 6:1 (E = 2.62 MPa), 9:1 (E = 1.95 MPa), and 17:1(E = 0.89 MPa). As the pyrene-labeled PS layer, where the local $T_{\rm g}(z)$ is measured, is moved closer to the PS/PDMS interface by decreasing the thickness of the neat PS z-layer (see Fig. $\overline{\mathbf{I}}$ a), the local $T_{\rm g}(z)$ decreases in an apparent linear fashion by tens of degrees Celsius from $T_{\rm g}^{\rm bulk}$ for PS, with an ≈ 40 K larger $T_{\rm g}(z)$ decrease for the softer PDMS underlayers. The distance $z \approx 65$ –90 nm from the PS/PDMS interface at which $T_{\rm g}^{\rm bulk}$ is recovered is significantly shorter than the $z\approx 225$ –250 nm observed previously for soft underlayers by Baglay et al. [16][17] for a series of weakly immiscible polymer pairs with interfacial widths $w_I = 5-7$ nm. We believe this difference is likely due to the greater immiscibility of PS/PDMS, whose interaction parameter χ is an order of magnitude larger

than the weakly immiscible systems studied previously, such that the interfacial width $w_I \sim \chi^{-1/2}$ for the PS/PDMS system would be much smaller. For PS/PDMS, we estimate the interfacial width $w_I = \frac{2b}{\sqrt{6\chi}} \approx 1.5$ nm from the interaction parameter $\chi = 0.17$ at 140 °C where the PS/PDMS interface is annealed to equilibrium (b is the statistical segment length) for a composition profile $\phi(z) = \frac{1}{2} \left[1 + \tanh\left(\frac{2z}{w_I}\right) \right]$. Supporting this conclusion is the recent theoretical work by Mirigian and Schweizer that demonstrated an approximate doubling of the length scale in interface perturbations by incorporating a larger, more realistic interfacial width for a polymer-air interface compared to the infinitely narrow, step-function interface most commonly employed by theoretical works. ⁵⁴ Unfortunately, theoretical difficulties and limited computational power make the modeling of polymerpolymer systems with large interfacial widths challenging.

Theoretical efforts aimed at understanding T_{g} perturbations near interfaces have suggested that local elastic stiffness 293055 or rigidity of the neighboring domain correlated with the Debye-Waller factor may be strong controlling parameters for affecting local alpha-relaxations. These efforts would suggest that the high-frequency, glassy shear modulus $G(\omega)$ would then be the relevant property for correlating with local $T_{\rm g}(z)$ shifts. However, varying the cross-link ratio of PDMS changes the zero-frequency, rubbery modulus of the elastomer, not the high-frequency glassy response. Tiwari et al. 47 showed using DMA that while the low-frequency elastomeric response changed with base-to-cross-linker ratio as shown in Fig. 2, the high frequency glassy Young's modulus $E(\omega)$ was the same for ratios of 10:1, 20:1, and 30:1, as would be expected for this level of cross-linking.

The most puzzling aspect of these $T_g(z)$ results is the enormous 40 K change in local $T_{\rm g}$ occurring within the PS domain for such a small change in underlying PDMS modulus, varying only from 0.9–2.6 MPa. From existing literature studies we know there are limitations over which we can extrapolate the modulus-dependent data shown in Fig. 3. As already mentioned, the PS/silica system with GPa underlayer modulus reports T_{σ}^{bulk} . However, even at the opposite extreme of PS films floating on top of liquid glycerol, the $T_{\rm g}(h)$ behavior has been reported to be identical to PS on silica. [56][57] If both extremely hard (GPa) and extremely soft (liquid) underlayers report no $T_{\rm g}$ perturbation from the underlying interface, how is it that intermediate (MPa) underlayers cause such a large shift in local $T_{\rm g}(z)$? One immediate difference is that both the PS/silica and PS/glycerol systems have sharp interfaces with widths ~ 0.5 nm only.

We have already identified that the large $T_{\rm g}(z)$ profiles require a broad, well-interpenetrated interface. However, this does not address why PDMS modulus values within the MPa range would be the region to impart such large shifts in local $T_{\rm g}(z)$. The pyrene dye identifies T_{g} on cooling as the temperature at which the local polymer matrix falls out of equilibrium as it passes from its rubbery plateau modulus ($E_{\rm R}=0.6~{\rm MPa}$ for ${\rm PS}^{58}$) through the glass transition to its glassy modulus $(E_{\rm G}=3.2~{\rm GPa}^{59})$, which might reasonably occur when the PS modulus is of order a few to tens of MPa, a value comparable to that of the underlying PDMS. In an earlier publication, 15 we introduced the idea that perhaps the coupling of local mobility across interfaces behaves in a manner analogous to impedance matching. In contrast to a sharp interface that would cause reflection of density waves (phonon modes), a sufficiently broad interface with also some amount of similarity in the mechanical properties on either side of the interface (e.g., density and modulus of the material that would impact the velocity of such acoustic waves) would allow for transmission of such waves across the interface changing the boundary conditions of phonon mode propagation throughout the material. How exactly such a change in phonon mode propagation translates into the measured local $T_{\rm g}(z)$ profiles is not quite clear at this point, but certainly much has been said in the literature associating phonon modes, so-called "soft spots", and alpha relaxations. 60161 Further work along these lines is underway.

Acknowledgements

The authors gratefully acknowledge support from the National Science Foundation Polymers Program (DMR-1709132 and DMR-1905782) and Emory University.

Supporting Information

Details of experimental procedures and control measurements (PDF).

REFERENCES

- Schweizer, K. S.; Simmons, D. S. Progress towards a phenomenological picture and theoretical understanding of glassy dynamics and vitrification near interfaces and under nanoconfinement. *Journal of Chemical Physics* 2019, 151, 240901.
- (2) Ediger, M. D.; Forrest, J. A. Dynamics near Free Surfaces and the Glass Transition in Thin Polymer Films: A View to the Future. *Macromolecules* **2014**, *47*, 471 478.
- (3) Vogt, B. D. Mechanical and viscoelastic properties of confined amorphous polymers. *Journal of Polymer Science Part B: Polymer Physics* **2018**, *56*, 9–30.

- (4) Ellison, C. J.; Torkelson, J. M. The distribution of glass-transition temperatures in nanoscopically confined glass formers. *Nature Materials* **2003**, 2, 695 – 700.
- (5) Roth, C. B.; McNerny, K. L.; Jager, W. F.; Torkelson, J. M. Eliminating the enhanced mobility at the free surface of polystyrene: Fluorescence studies of the glass transition temperature in thin bilayer films of immiscible polymers. *Macro*molecules 2007, 40, 2568 – 2574.
- (6) Roth, C. B.; Torkelson, J. M. Selectively probing the glass transition temperature in multilayer polymer films: Equivalence of block copolymers and multilayer films of different homopolymers. *Macromolecules* 2007, 40, 3328 3336.
- (7) Yoon, H.; McKenna, G. B. Substrate effects on glass transition and free surface viscoelasticity of ultrathin polystyrene films. *Macromolecules* **2014**, 47, 8808 8818.
- (8) Lang, R. J.; Merling, W. L.; Simmons, D. S. Combined dependence of nanoconfined Tg on interfacial energy and softness of confinement. ACS Macro Letters 2014, 3, 758 762.
- (9) Evans, C. M.; Narayanan, S.; Jiang, Z.; Torkelson, J. M. Modulus, Confinement, and Temperature Effects on Surface Capillary Wave Dynamics in Bilayer Polymer Films Near the Glass Transition. *Physical Review Letters* **2012**, *109*, 038302.
- (10) Evans, C. M.; Kim, S.; Roth, C. B.; Priestley, R. D.; Broadbelt, L. J.; Torkelson, J. M. Role of neighboring domains in determining the magnitude and direction of Tg-confinement effects in binary, immiscible polymer systems. *Polymer* 2015, 80, 180 187.
- (11) Sharma, R. P.; Green, P. F. Role of "Hard" and "Soft" Confinement on Polymer Dynamics at the Nanoscale. *ACS Macro Letters* **2017**, *6*, 908 914.
- (12) Jo, K.-I.; Oh, Y.; Sung, B. J.; Kim, T.-H.; Um, M. S.; Choi, W. J.; Bang, J.; Yuan, G.; Satija, S. K.; Koo, J. Enhanced Dynamics of Confined Polymers near the Immiscible Polymer-Polymer Interface: Neutron Reflectivity Studies. ACS Macro Letters 2020, 9, 210-215.
- (13) Hsu, D. D.; Xia, W.; Song, J.; Keten, S. Dynamics of interacting interphases in polymer bilayer thin films. *MRS Communications* **2017**, *7*, 832–839.
- (14) Mani, S.; Khare, R. Effect of Chain Flexibility and Interlayer Interactions on the Local Dynamics of Layered Polymer Systems. *Macromolecules* 2018, 51, 576–588.
- (15) Rauscher, P. M.; Pye, J. E.; Baglay, R. R.; Roth, C. B. Effect of adjacent rubbery layers on the physical aging of glassy polymers. *Macro-molecules* 2013, 46, 9806 – 9817.
- (16) Baglay, R. R.; Roth, C. B. Communication: Experimentally determined profile of local glass transition temperature across a glassy-rubbery polymer interface with a Tg difference of 80 K. Journal of Chemical Physics 2015, 143, 111101.

- (17) Baglay, R. R.; Roth, C. B. Local glass transition temperature Tg(z) of polystyrene next to different polymers: Hard vs. soft confinement. *Journal of Chemical Physics* 2017, 146, 203307.
- (18) Baglay, R. R.; Roth, C. B. Experimental Study of the Influence of Periodic Boundary Conditions: Effects of Finite Size and Faster Cooling Rates on Dissimilar Polymer–Polymer Interfaces. ACS Macro Letters 2017, 6, 887 – 891.
- (19) Lee, J.-H.; Veysset, D.; Singer, J. P.; Retsch, M.; Saini, G.; Pezeril, T.; Nelson, K. A.; Thomas, E. L. High strain rate deformation of layered nanocomposites. *Nature Communications* **2012**, *3*, 1164.
- (20) Shen, L.; Wang, T.-P.; Lin, F.-Y.; Torres, S.; Robison, T.; Kalluru, S. H.; Hernández, N. B.; Cochran, E. W. Polystyrene-block-Polydimethylsiloxane as a Potential Silica Substitute for Polysiloxane Reinforcement. ACS Macro Letters 2020, 9, 781–787.
- (21) Beltramo, P. J.; Schneider, D.; Fytas, G.; Furst, E. M. Anisotropic Hypersonic Phonon Propagation in Films of Aligned Ellipsoids. *Physical Review Letters* 2014, 113, 205503.
- (22) Bates, F. S.; Hillmyer, M. A.; Lodge, T. P.; Bates, C. M.; Delaney, K. T.; Fredrickson, G. H. Multiblock Polymers: Panacea or Pandora's Box? Science 2012, 336, 434 – 440.
- (23) Liu, R. Y. F.; Bernal-Lara, T. E.; Hiltner, A.; Baer, E. Polymer Interphase Materials by Forced Assembly. *Macromolecules* 2005, 38, 4819–4827.
- (24) Kang, E.; Graczykowski, B.; Jonas, U.; Christie, D.; Gray, L. A. G.; Cangialosi, D.; Priestley, R. D.; Fytas, G. Shell Architecture Strongly Influences the Glass Transition, Surface Mobility, and Elasticity of Polymer Core-Shell Nanoparticles. *Macromolecules* 2019, 52, 5399 – 5406.
- (25) Tao, Y.; Kim, J.; Torkelson, J. M. Achievement of quasi-nano structured polymer blends by solidstate shear pulverization and compatibilization by gradient copolymer addition. *Polymer* 2006, 47, 6773 – 6781.
- (26) Kasavan, B. L.; Baglay, R. R.; Roth, C. B. Local Glass Transition Temperature $T_{\rm g}(z)$ Profile in Polystyrene next to Polybutadiene with and without Plasticization Effects. *Macromolecular Chemistry and Physics* **2018**, 219, 1700328.
- (27) Huang, X.; Roth, C. B. Optimizing the Grafting Density of Tethered Chains to Alter the Local Glass Transition Temperature of Polystyrene near Silica Substrates: The Advantage of Mushrooms over Brushes. ACS Macro Letters 2018, 7, 269—274
- (28) Huang, X.; Thees, M. F.; Size, W. B.; Roth, C. B. Experimental Study of Substrate Roughness on the Local Glass Transition of Polystyrene. *Jour*nal of Chemical Physics 2020, 152, 244901.
- (29) Phan, A. D.; Schweizer, K. S. Theory of the spatial transfer of interface-nucleated changes of dy-

- namical constraints and its consequences in glass-forming films. *Journal of Chemical Physics* **2019**, 150, 044508.
- (30) Phan, A. D.; Schweizer, K. S. Theory of Spatial Gradients of Relaxation, Vitrification Temperature and Fragility of Glass-Forming Polymer Liquids Near Solid Substrates. ACS Macro Letters 2020, 9, 448–453.
- (31) Simmons, D. S. An Emerging Unified View of Dynamic Interphases in Polymers. *Macromolecular Chemistry And Physics* **2016**, *217*, 137 148.
- (32) Tito, N. B.; Lipson, J. E. G.; Milner, S. T. Lattice model of mobility at interfaces: free surfaces, substrates, and bilayers. *Soft Matter* **2013**, *9*, 9403 9413.
- (33) DeFelice, J.; Milner, S. T.; Lipson, J. E. G. Simulating Local Tg Reporting Layers in Glassy Thin Films. *Macromolecules* **2016**, *49*, 1822 1833.
- (34) Hanakata, P. Z.; Betancourt, B. A. P.; Douglas, J. F.; Starr, F. W. A unifying framework to quantify the effects of substrate interactions, stiffness, and roughness on the dynamics of thin supported polymer films. *Journal of Chemical Physics* 2015, 142, 234907.
- (35) Stafford, C. M.; Vogt, B. D.; Harrison, C.; Julthongpiput, D.; Huang, R. Elastic moduli of ultrathin amorphous polymer films. *Macromolecules* **2006**, *39*, 5095 5099.
- (36) Stafford, C. M.; Harrison, C.; Beers, K. L.; Karim, A.; Amis, E. J.; Vanlandingham, M. R.; Kim, H. C.; Volksen, W.; Miller, R. D.; Simonyi, E. E. A buckling-based metrology for measuring the elastic moduli of polymeric thin films. Nature Materials 2004, 3, 545 – 550.
- (37) Torres, J. M.; Stafford, C. M.; Vogt, B. D. Elastic Modulus of Amorphous Polymer Thin Films: Relationship to the Glass Transition Temperature. *ACS Nano* **2009**, *3*, 2677 – 2685.
- (38) Kriisa, A.; Park, S. S.; Roth, C. B. Characterization of phase separation of polystyrene/poly(vinyl methyl ether) blends using fluorescence. *Journal of Polymer Science Part B: Polymer Physics* **2012**, 50, 250 256.
- (39) Huang, X.; Roth, C. B. Changes in the temperature-dependent specific volume of supported polystyrene films with film thickness. *Journal of Chemical Physics* **2016**, *144*, 234903.
- (40) Wilder, E. A.; Guo, S.; Lin-Gibson, S.; Fasolka, M. J.; Stafford, C. M. Measuring the Modulus of Soft Polymer Networks via a Buckling-Based Metrology. *Macromolecules* 2006, 39, 4138 4143.
- (41) Kalyanasundaram, K.; Thomas, J. K. Environmental Effects on Vibronic Band Intensities in Pyrene Monomer Fluorescence and Their Application in Studies of Micellar Systems. *Journal of* the American Chemical Society 1977, 99, 2039 – 2044.
- (42) Valeur, B. Molecular Fluorescence: Principles and Applications; Wiley-VCH: Weinheim, 2002.

- (43) Kim, S.; Hewlett, S. A.; Roth, C. B.; Torkelson, J. M. Confinement effects on glass transition temperature, transition breadth, and expansivity: Comparison of ellipsometry and fluorescence measurements on polystyrene films. *European Physical Journal E* **2009**, 30, 83 92.
- (44) Glover, J. D.; McLaughlin, C. E.; McFarland, M. K.; Pham, J. T. Extracting uncrosslinked material from low modulus Sylgard 184 and the effect on mechanical properties. *Journal of Polymer Science* 2020, 58, 343–351.
- (45) Carrillo, F.; Gupta, S.; Balooch, M.; Marshall, S. J.; Marshall, G. W.; Pruitt, L.; Puttlitz, C. M. Nanoindentation of polydimethylsiloxane elastomers: Effect of crosslinking, work of adhesion, and fluid environment on elastic modulus. *Journal of Materials Research* 2005, 20, 2820–2830.
- (46) Trappmann, B.; Gautrot, J. E.; Connelly, J. T.; Strange, D. G. T.; Li, Y.; Oyen, M. L.; Stuart, M. A. C.; Boehm, H.; Li, B.; Vogel, V.; Spatz, J. P.; Watt, F. M.; Huck, W. T. S. Extracellular-matrix tethering regulates stem-cell fate. *Nature Materials* 2012, 11, 642–649.
- (47) Tiwari, A.; Dorogin, L.; Bennett, A. I.; Schulze, K. D.; Sawyer, W. G.; Tahir, M.; Heinrich, G.; Persson, B. N. J. The effect of surface roughness and viscoelasticity on rubber adhesion. Soft Matter 2017, 13, 3602 – 3621.
- (48) Schott Corporation, Technical Information Advanced Optics 31: Mechanical and Thermal Properties of Optical Glass; version October 2018.
- (49) Torres, J. M.; Stafford, C. M.; Vogt, B. D. Impact of molecular mass on the elastic modulus of thin polystyrene films. *Polymer* **2010**, *51*, 4211 4217.
- (50) Forrest, J. A.; Dalnoki-Veress, K. Sub-glass-transition temperature interface formation between an immiscible glass rubber pair. *Journal of Polymer Science Part B: Polymer Physics* **2001**, 39, 2664 2670.
- (51) Lee, J. N.; Jiang, X.; Ryan, D.; Whitesides, G. M. Compatibility of Mammalian Cells on Surfaces of Poly(dimethylsiloxane). *Langmuir* 2004, 20, 11684–11691.
- (52) Melillo, M. J. PDMS Network Structure-Property Relationships: Influence of Molecular Architecture on Mechanical and Wetting Properties; Ph.D. Dissertation, North Carolina State University, 2017.
- (53) Eitouni, H. B.; Balsara, N. P. In *Physical Properties of Polymers Handbook*, 2nd ed.; Mark, J. E., Ed.; Springer: New York, 2007; Chapter 19, pp 339–356.
- (54) Mirigian, S.; Schweizer, K. S. Influence of chemistry, interfacial width, and non-isothermal conditions on spatially heterogeneous activated relaxation and elasticity in glass-forming free standing films. *Journal of Chemical Physics* 2017, 146, 203301.
- (55) Mirigian, S.; Schweizer, K. S. Communication:

- Slow relaxation, spatial mobility gradients, and vitrification in confined films. *Journal of Chemical Physics* **2014**, *141*, 161103.
- (56) Wang, J.; McKenna, G. B. Viscoelastic and Glass Transition Properties of Ultrathin Polystyrene Films by Dewetting from Liquid Glycerol. *Macro-molecules* 2013, 46, 2485–2495.
- (57) Wang, J.; McKenna, G. B. A novel temperaturestep method to determine the glass transition temperature of ultrathin polymer films by liquid dewetting. *Journal of Polymer Science Part B: Polymer Physics* **2013**, *51*, 1343–1349.
- (58) Hiemenz, P. C.; Lodge, T. P. *Polymer Chemistry*, 2nd ed.; CRC Press: Boca Raton, FL, 2007.
- (59) Brandrup, J., Immergut, E. H., Grulke, E. A., Abe, A., Bloch, D. H., Eds. *Polymer Handbook*, 4th ed.; Wiley: New York, 1999.
- (60) Smessaert, A.; Rottler, J. Structural Relaxation in Glassy Polymers Predicted by Soft Modes: A Quantitative Analysis. Soft Matter 2014, 10, 8533–8541.
- (61) Manning, M. L.; Liu, A. J. Vibrational Modes Identify Soft Spots in a Sheared Disordered Packing. *Physical Review Letters* 2011, 107, 108302.

Supporting Information:

Local Glass Transition Temperature $T_{ m g}(z)$ Within Polystyrene Is Strongly Impacted by the Modulus of the Neighboring PDMS Domain

Yannic J. Gagnon and Connie B. Roth*

Department of Physics, Emory University, Atlanta, Georgia, 30322 USA *To whom correspondence should be addressed. Email: cbroth@emory.edu

Experimental Methods

High molecular weight pyrene-labeled polystyrene (PS-Py) with 1.4 mol\% pyrene ($M_{\rm w}$ = 672 kg/mol, $M_{\rm w}/M_{\rm n}=1.3$) was synthesized using free radical copolymerization of styrene with 1-pyrenylbutyl methacrylate at 50 °C for 24 h under a nitrogen environment using azobisisobutyronitrile (AIBN) as initiator as described in Refs. 16,38. Unlabeled (neat) polystyrene (PS) ($M_{\rm w}=1920~{\rm kg/mol},~M_{\rm w}/M_{\rm n}=1.26$) was purchased from Pressure Chemical and used as received. The polydimethylsiloxane (PDMS) layers were made from Dow Corning's Sylgard 184 elastomer kit. Cross-linked PDMS of varying modulus was made by mixing the base prepolymer with the curing agent at different ratios n:1 between 6:1 and 17:1 by weight. The mixture was stirred with a metal spatula for 30 s and then left to sit for 30 min to remove air bubbles introduced during mixing. The PDMS mixture was then poured into a mold formed between two glass microscope slides separated by an aluminum foil spacer of thickness 200–215 μ m with a rectangular opening of 1.5 cm \times 4 cm. A Teflon sheet was added between the top of the PDMS sample and the upper glass slide for ease of opening the mold after the PDMS was cured. Binder clips were placed on all four sides to secure the mold. Curing of the PDMS was done in an oven at 70 °C for 2 h to match the curing conditions of Refs. 35.40. After curing, a scalpel was used to slice a 1.5 cm \times 1.5 cm square section of the PDMS layer and place it onto the quartz slide used for fluorescence measurements. PDMS layer thicknesses ranged between 50 μ m and 180 μ m, as measured by a micrometer. Much thinner PDMS layers were also made by spin-coating the PDMS mixture prior to curing resulting in thicknesses of only 2 μ m, as measured by ellipsometry. The local $T_{\rm g}(z=50~{\rm nm})$ values within PS were the same for spin-coated PDMS underlayers as for the mold cast PDMS, demonstrating that the measured $T_{\rm g}(z)$ profile is independent of PDMS layer thickness within this range of 2–180 μ m.

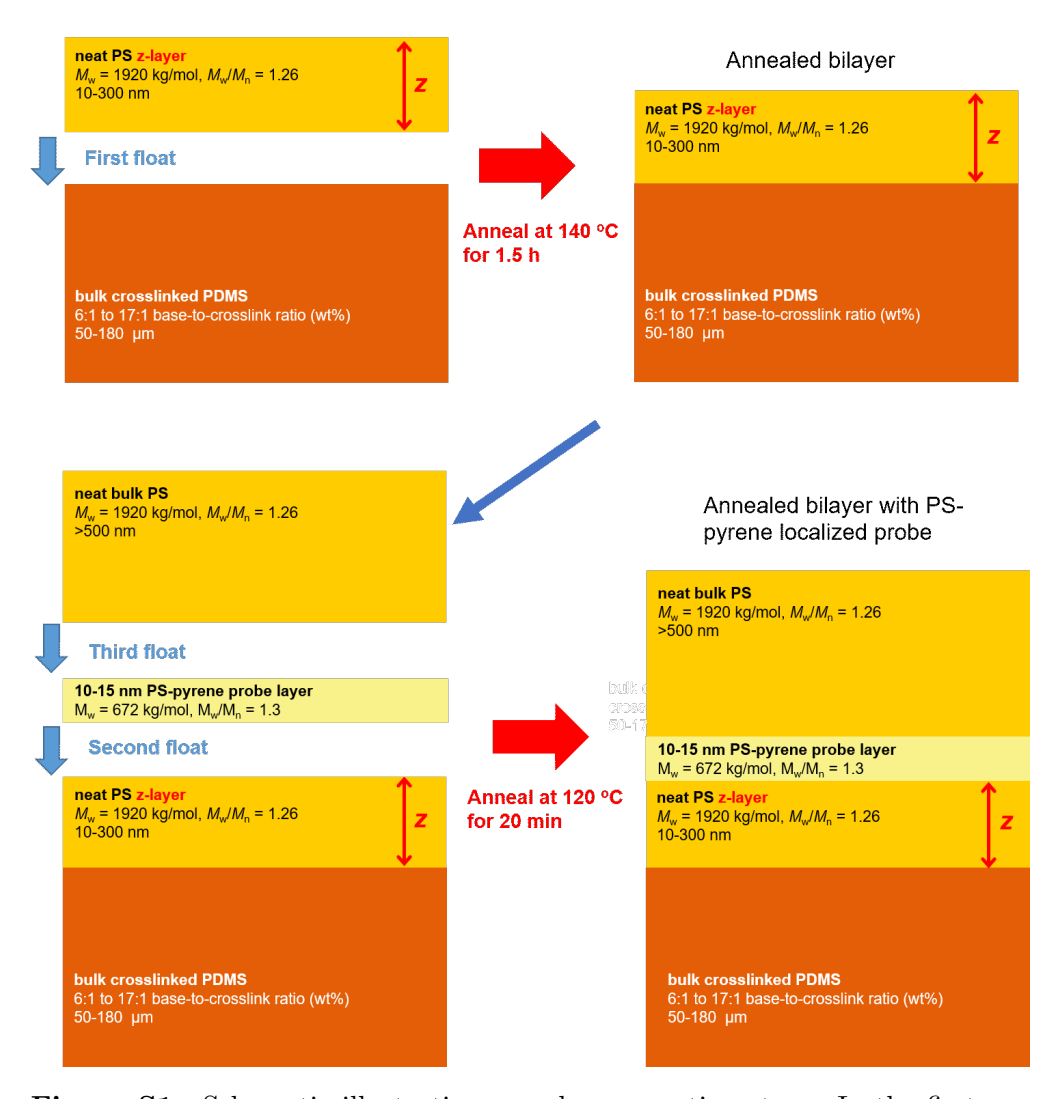


Figure S1. Schematic illustrating sample preparation steps. In the first annealing step, the PS z-layer and PDMS underlayer are annealed at 140 °C for 1.5 h to ensure this dissimilar polymer-polymer interface is annealed to equilibrium. The remaining PS-Py probe and bulk PS layers are then added, with a final annealing step of 20 min at 120 °C done prior to the start of the fluorescence measurements to consolidate all the layers into a single material with no air gaps, while keeping the PS-Py probe layer localized at a position z from the PS/PDMS interface.

Figure S1 illustrates the individual layers and steps used to construct the multilayer sample geometry used. PS and PS-Py layers were made by spin-coating films from toluene solutions onto freshly-cleaved mica, varying spin speed and solution concentration to obtain films of the desired thicknesses. All PS and PS-Py layers were annealed individually on mica at 120 °C under vacuum for a minimum of 14 h to remove residual solvent and release any stresses imparted during the spin-coating process. Multilayer samples were then assembled by floating the individual films onto room temperature deionized water and capturing the layers from below with the portion of the sample already assembled. Between each floating step, the sample was allowed to thoroughly dry under an incandescent lamp. The top bulk PS layers were made >500 nm thick to ensure that the PS-Py layer would be unaffected by free surface effects. Annealing of the layers to create a consolidated sample with no air gaps was done in two stages to ensure that equilibrium chain interpenetration across the PS/PDMS interface was obtained, while minimizing interdiffusion of the PS-Py probe layer. ISII As shown in Fig. S1, the PS z- and PDMS layers were first annealed separately at 140 °C for 1.5 h, prior to floating the PS-Py and bulk PS layers on top. A final annealing step at 120 °C for 20 min was then done immediately prior to the start of the fluorescence measurements.

Layer thicknesses were determined using a variable angle spectroscopic ellipsometer with rotating compensator (J.A. Woollam M-2000). The amplitude ratio $\Psi(\lambda)$ and phase shift $\Delta(\lambda)$ of the ratio of p- to s-polarized light Fresnel reflection coefficients were measured at three angles of incidence, 55°, 60°, and 65°, for wavelengths λ spanning 400–1000 nm. The film thickness h and wavelength-dependent index of refraction $n(\lambda)$ of the polymer layer were determined by fitting the $\Psi(\lambda)$ and $\Delta(\lambda)$ data using Woollam's WVASE software to an optical layer model composed of a transparent Cauchy layer $n(\lambda) = A + \frac{B}{\lambda^2} + \frac{C}{\lambda^4}$ for the polymer film, and a 2.0 nm native oxide layer atop a semi-infinite silicon substrate. For the 2 μ m thick PDMS films, an additional thickness non-uniformity parameter, typically between 3% and 7%, was modeled in the CompleteEASE software. PDMS Cauchy parameter values

obtained were A = 1.406, $B = 0.00251 \ \mu\text{m}^2$, and $C = 0.00016 \ \mu\text{m}^4$, in good agreement with values reported in the literature [1].

Fluorescence measurements were done using a Photon Technology International QuantaMaster spectrofluorometer following the protocol outlined in Refs. [15-17] Samples were placed in a Peltier-cooled Instec TS62 heat stage with dry nitrogen gas continuously flowed through the chamber at 1.1 L/min to prevent condensation of moisture below room temperature. The pyrene dye was excited at a wavelength of 330 nm using a xenon arc lamp with an excitation band-pass of 5.5-6.0 nm and an emission band-pass of 5.0 nm. Fluorescence measurements were initiated by heating the sample to the starting temperature, typically 120 °C, and equilibrating the sample for 20 min as the final annealing step. While cooling the sample at 1 °C/min, the fluorescence intensity of pyrene was monitored at an emission wavelength of 379 nm for 3 s every 27 s, as described previously. At the end of each measurement run, the sample was reheated to the starting temperature to ensure that the same emission intensity was obtain at 120 °C, verifying that photobleaching was negligible and the sample had remained stable.

The $T_{\rm g}$ value for a given run was determined from the change in slope of the fluorescence intensity I with temperature T by performing linear fits to the I(T) data above and below the transition, and then identifying the temperature at which the two linear fits intersected. Figure S2 shows three such intensity vs. temperature curves for the 9:1 PDMS cross-link ratio for samples with the pyrene-labeled layer placed at different distances from the PS/PDMS interface: z=33, 53, 146 nm. The data ranges for the linear fits were chosen to begin at a minimum of 5 °C from the transition temperature and to include the largest amount of data, while maximizing the R^2 value for the fits. In Fig. S2, the measured $T_{\rm g}(z)$ values systematically decreased with decreasing z as the PS/PDMS interface was approached, with $T_{\rm g}^{\rm bulk}$ being recovered sufficiently far ($z \geq 100$ nm) from the interface. As in our previous fluorescence studies of the local $T_{\rm g}(z)$ as a function of position from an interface, only a single $T_{\rm g}$ value was found for a given z value no matter how wide the temperature range inves-

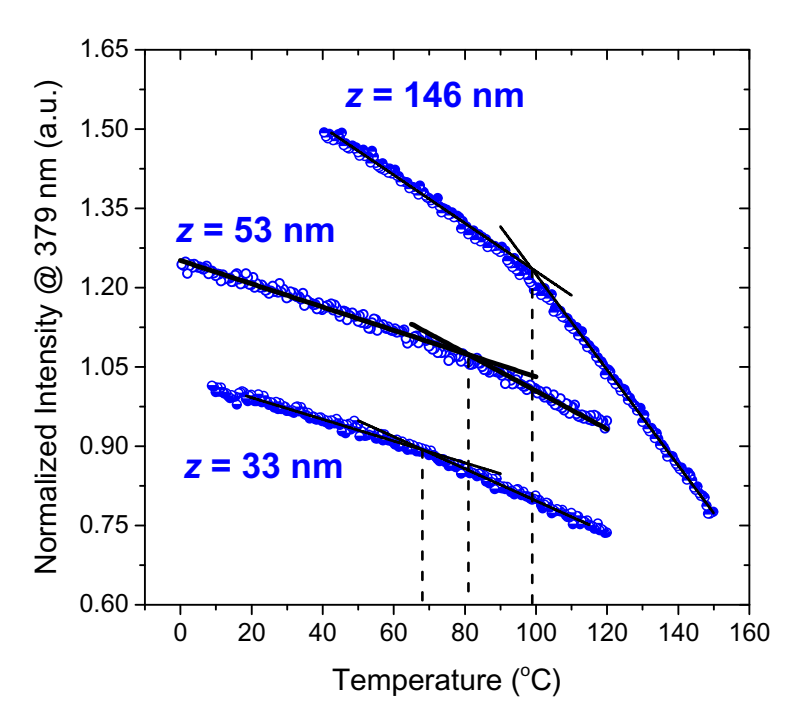


Figure S2. Temperature dependent fluorescence intensity measured for three different PS/PDMS multilayer samples with the 9:1 PDMS cross-link ratio where the pyrene-labeled layer was placed at varying distances z from the PS/PDMS interface resulting in local $T_{\rm g}(z)$ values measured within the PS domain of $T_{\rm g}(z=146~{\rm nm})=99~{\rm ^{\circ}C}$ (equivalent to $T_{\rm g}^{\rm bulk}$), $T_{\rm g}(z=53~{\rm nm})=81~{\rm ^{\circ}C}$, and $T_{\rm g}(z=33~{\rm nm})=68~{\rm ^{\circ}C}$.

tigated. Tell72627 As initially demonstrated by Ellison and Torkelson, the change in pyrene fluorescence intensity with temperature is sensitive to the stiffness (thermal expansion) of the surrounding polymer matrix, where the $T_{\rm g}$ values measured by fluorescence for polymer films of a given thickness h are in excellent agreement with $T_{\rm g}(h)$ values measured by ellipsometry, as well as onset $T_{\rm g}$ values measured by differential scanning calorimetry (DSC) for thick (bulk) films. The bulk glass transition temperature $T_{\rm g}^{\rm bulk} = 101.5 \pm 2.0$ °C shown as horizontal dotted lines in Figs. and were determined from the average of local $T_{\rm g}(z)$ values with $z \geq 100$ nm.

From our 2017 study on weakly immiscible polymers, \Box we learned that the broad $T_{\rm g}(z)$ profile showing dynamical coupling across dissimilar polymer domains only develops upon annealing of the dissimilar polymer-polymer interface to equilibrium. To determine the annealing conditions necessary to obtain an equilibrium PS/PDMS interface, measurements

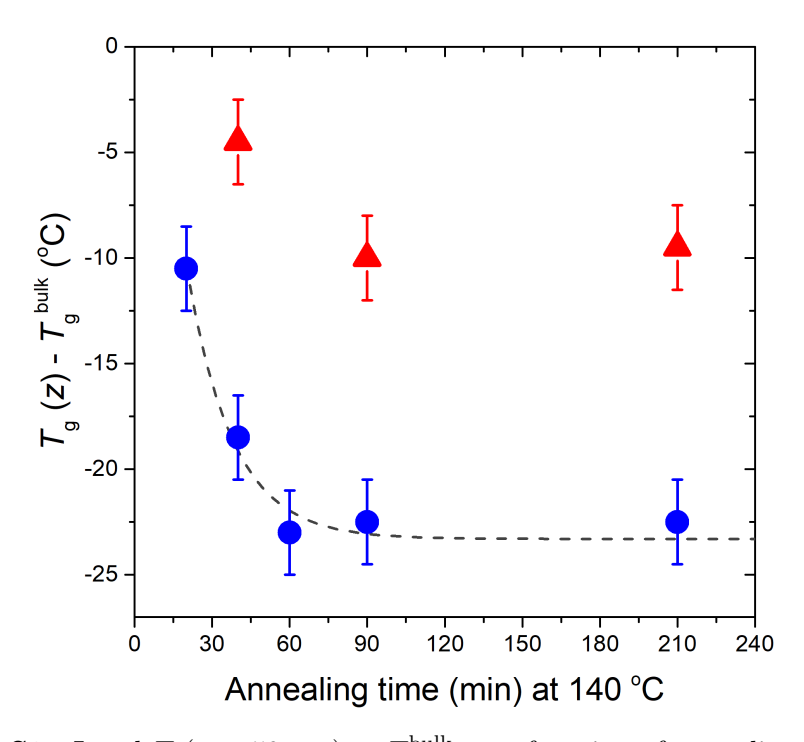


Figure S3. Local $T_{\rm g}(z=50~{\rm nm})-T_{\rm g}^{\rm bulk}$ as a function of annealing time at 140 °C of the PS/PDMS interface (first annealing stage). Solid blue circles are for samples made with 9:1 PDMS, while the solid red triangles are for samples made with 6:1 PDMS. The dashed curve is an exponential decay fit to the 9:1 data. The $T_{\rm g}(z=50~{\rm nm})$ value stabilizes after 60–90 min of annealing as the PS/PDMS interface reaches equilibrium.

of the local $T_{\rm g}(z=50~{\rm nm})$ were done on samples where the annealing time of the first annealing step at 140 °C (see Fig. S1) was increased from 20 to 210 min. Figure S3 shows how the local $T_{\rm g}(z=50~{\rm nm})$, relative to $T_{\rm g}^{\rm bulk}$, decreases upon annealing of the PS/PDMS interface, stabilizing after 60–90 min as the PS/PDMS interface reaches equilibrium. Data shown are for samples made with either 9:1 or 6:1 PDMS cross-linking ratios. From these results we concluded that 90 min of annealing at 140 °C during the first annealing step of the sample assembly process shown in Fig. S1 is sufficient and necessary to obtain reproducible and reliable $T_{\rm g}(z)$ values for the PS/PDMS samples.

We estimate the equilibrium interfacial width w_I attained between PS and PDMS annealed at 140 °C based on values of the interaction parameter χ from the literature evaluated at 140 °C. From values tabulated by Eitouni and Balsara in Mark's *Physical Properties of*

Polymers Handbook, 53

$$\chi(T) = A + \frac{B}{T} \tag{S1}$$

for PS/PDMS with A = 0.031 and B = 58 K based on measurements from 165–225 °C of the order-disorder-transition temperature (T_{ODT}) for block copolymers by Ref. [2], where values have been adjusted by Eitouni and Balsara to account for a common reference volume. Based on eq. [51] with a minor temperature extrapolation, $\chi(T) = 0.17$ at 140 °C. The interfacial width w_I for two high molecular weight polymers with similar statistical segment lengths b and densities is given by [3]

$$w_I = \frac{2b}{\sqrt{6\chi}},\tag{S2}$$

for a composition profile

$$\phi(z) = \frac{1}{2} \left[1 + \tanh\left(\frac{2z}{w_I}\right) \right]. \tag{S3}$$

Taking the average of the statistical segment lengths for PS and PDMS, $b_{PS} = 0.67$ nm and $b_{PDMS} = 0.58$ nm, eq. 2 gives $w_I = 1.24$ nm. Such calculations of interfacial widths based on χ parameters often provide underestimates of w_I compared with experimentally measured values because real polymer-polymer interfaces are also broadened by interface roughening associated with capillary waves [3]. We note that the light cross-linking of the PDMS elastomer may also result in minor differences to the interfacial width. Based on these considerations, we estimate the PS/PDMS interfacial width as $w_I \approx 1.5$ nm.

To ensure that our $T_{\rm g}(z)$ results were not influenced by any unreacted PDMS material migrating from the PDMS to the PS domain, we also performed $T_{\rm g}(z)$ measurements for samples where the PDMS layers underwent a washing procedure of soaking the PDMS in good solvent to remove unreacted material. PDMS strips with masses between 5–10 mg and thicknesses between 50–200 μ m were soaked for 24 h in 200 mL of toluene, a good solvent for PDMS. The strips were then degassed and reweighed to determine the mass lost, where we also verified that further washing did not result in additional mass loss. The resulting gel fraction, corresponding to the amount of polymer participating in the network,

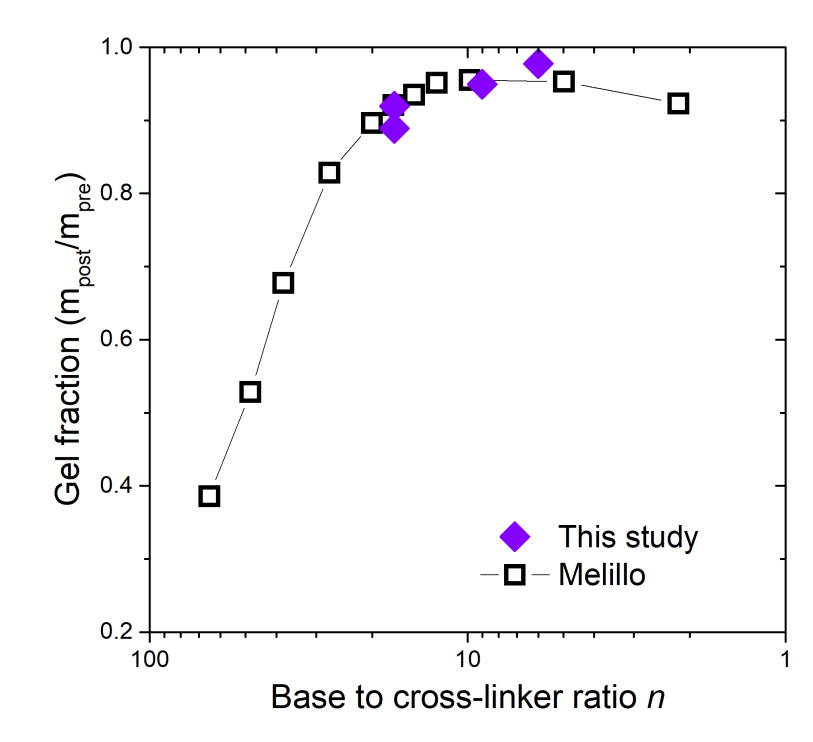


Figure S4. Gel fraction $\frac{m_{\text{post}}}{m_{\text{pre}}}$ determined from measurements of the mass lost after Sylgard 184 PDMS was soaked in toluene, a good solvent, for 24 h. Data from Ref. 52 using Soxhlet extraction are also shown. Good agreement is observed with mass losses of 2%-10% for the base:cross-linker range of 6:1-17:1 used in this study.

was determined from the ratio of the mass measured post- and pre-soaking $\frac{m_{\text{post}}}{m_{\text{pre}}}$ [4]. In Figure S4 we plot our measured gel fraction values together with those from Melillo, where the removal of unreacted material from Sylgard 184 PDMS was done via Soxhlet extraction with toluene over 24 h on PDMS that had been cured at 70 °C for 24 h. Our measured gel fractions ranged from 0.90 to 0.98 for PDMS made with ratios of 17:1, 9:1, and 6:1, in good agreement with those from Ref. 52. Using dynamic mechanical analysis (DMA), Melillo reported no change in the storage and loss moduli between the pre- and post-extracted PDMS for the base:cross-linker range of 6:1–17:1 used in our study. As shown in Figures 3 and 4 denoted with X-symbols, the measured $T_g(z)$ values were the same for samples where the PDMS had been soaked in good solvent to remove unreacted material.

Additional References*

- *Superscripted references correspond to those listed in the main text.
- [1] Spaeth, K.; Kraus, G.; Gauglitz, G. In-situ characterization of thin polymer films for applications in chemical sensing of volatile organic compounds by spectroscopic ellipsometry. Fresenius' Journal of Analytical Chemistry 1997, 357, 292–296.
- [2] Cochran, E. W.; Morse, D. C.; Bates, F. S. Design of ABC Triblock Copolymers near the ODT with the Random Phase Approximation. *Macromolecules* **2003**, *36*, 782–792.
- [3] Jones, R. A. L.; Richards, R. W. *Polymers at Surfaces and Interfaces*; Cambridge University Press, 1999.
- [4] Nandi, S.; Winter, H. H. Swelling Behavior of Partially Cross-Linked Polymers: A Ternary System. *Macromolecules* **2005**, *38*, 4447–4455.